Supplement of Atmos. Meas. Tech., 18, 2573–2590, 2025
https://doi.org/10.5194/amt-18-2573-2025-supplement

Atmospheric Measurement Techniques
Open Access

Supplement of

In-flight estimation of instrument spectral response functions using sparse representations

Jihanne El Haouari et al.

Correspondence to: Jihanne El Haouari (jihanne.elhaouari@prd.tesa.fr)

S1 Content of the supplementary materials

This document serves as supplementary material to the article (El Haouari et al., 2024), which introduces a novel sparse representation-based method for estimating Instrument Spectral Response Functions (ISRFs) and compares its performance to Gaussian and Super-Gaussian parametric models. The Supplement provides additional results demonstrating the proposed method adapts with no difficulty to other instruments; specifically, results are reported for the Avantes, GOME-2, OMI, and Tropomi spectrometers, described in Section S2. Results are presented in Section S3.

S2 Instruments, datasets & preprocessing

The proposed ISRF estimation method applied for data from the instruments Avantes, GOME-2, OMI and TROPOMI. The characteristics of the different instruments are displayed in Table S1. For each instrument, the ISRFs used are generated based on the dataset associated with each instruments. Then, to identify the ISRFs at the missing nominal wavelengths λ_l, a linear interpolation between two specified nominal wavelengths λ_a and λ_b with known ISRFs was employed and the obtained ISRF is defined by: $I_l = \frac{\lambda_l - \lambda_a}{\lambda_b - \lambda_a} I_b + \frac{\lambda_b - \lambda_l}{\lambda_b - \lambda_a} I_a$ and interpolated using splines to generate ISRFs with N_λ wavelengths and a sample size N. Note that the number N_λ of used wavelengths may differ from the number of pixels of the instrument, a situation that occurs when the ISRFs associated with the first and/or last pixels are not available.

Table S1. Characteristics of the instruments Avantes, GOME-2, OMI and TROPOMI.

	Instruments considered			
Characteristics	Avantes	GOME-2	OMI	TROPOMI
Number of spectral pixels	2048	- 4 channels - 4 detectors 1024 pixels	- 2 CCD detectors 1024 pixels	4 spectrometers 4 detectors
Wavelength ranges	UV,VIS,NIR (296-459nm)	UV (240-790nm)	UV(UV1-270-310nm, UV2:310-380nm) VIS(350-500nm)	UV (270-320nm) UVIS(320-500nm) NIR(675-775nm) SWIR(2305-2385nm)
Resolution	0.09-20nm	0.26 to 0.51nm	0.5nm	0.45-0.5nm 0.45-0.65nm 0.35-0.45nm 0.225-0.227nm
Number of wavelengths N_λ	1741	877 (third band (397-604-nm))	750 (VIS band)	994 (UVIS band (305-499nm))
ISRF sampling size N	199	705	299	257

S2.1 Avantes

Avantes (Ava) is an ultra-low straylight fiber spectrometer. The data used for this spectrometer was measured in April 2015 and 7 ISRFs were made available in the supplement material of (Beirle et al., 2017).

S2.2 GOME-2

The Global Ozone Monitoring Experiment-2 (GOME-2) is an optical spectrometer that was launched in the Metop-A EUMETSAT satellite in october 2006. All the information on the design and characterization of the spectrometer are described in (Munro et al., 2016). The aim of the GOME-2 mission is to obtain information on trace gas concentration by sensing the

Earth's backscattered radiance in the UV part of the spectrum (240-790 nm). Data for the ISRFs were made available by EUMETSAT[1]. The ISRFs were obtained in January 2007 using the FM3 model (Siddans and Latter, 2018).

S2.3 OMI

The Ozone Monitoring Instrument (OMI) is an hyperspectral imager onboard the NASA's Earth Observing system satellite Aura launched in July 2004. The aim of the mission is to determine trace gases at high spectral and spatial resolutions in both the atmosphere and troposphere, in order to determine the Earth's atmospheric composition and have a long global ozone record. The OMI slit functions were determined from preflight characterization for each spectral pixel (Sun et al., 2017). The ISRFs of the OMI spectrometer can be found for the UV-2 and VIS bands in the data product[2] of the KNMI Projects made in 2014 in KNMI, De Bilt, The Netherlands. The slit functions of the spectrometer are obtained by averaging the rows 17 to 47 and are derived from the parameterization described in RP-OMIE-KNMI-704. More information on the instrument calibration can be found in (Dobber et al., 2006) and in-flight performance was assessed in (Schenkeveld et al., 2017).

S2.4 TROPOMI

The Tropospheric Monitoring Instrument (TROPOMI) was launched on the Sentinel-5 Precursor Satellite in October 2017. The instrument is part of the new generation of atmospheric sounding instruments and was designed to continue GOME-2, SCIAMACHY and OMI missions with higher spatial and spectral resolutions (Kleipool et al., 2018). The ISRFs are first determined during extensive on-ground calibration campaign (van Hees et al., 2018) and were then expressed as a convolution between a normal distribution and a uniform distribution. The ISRFs considered in this work were extracted from the TROPOMI Calibration Key Data files whose third version was created in 2018 by KNMI for UV-VIS-NIR spectral bands and in 2016 by SRON for the SWIR band. More details on the data are described in (Smeets et al., 2002). More information about the spectrometer can be found in (Babic et al., 2022).

S3 Results and discussion

The performance evaluation of the various ISRF estimation methods is carried out in the same manner as described in Sections 5.2 and 5.3.1 of the manuscript.

S3.1 Illustration of single ISRF

Examples of ISRFs and their estimates are displayed in Fig. S1. First, it is interesting to note that the ISRF shapes can be significantly different depending on the considered wavelength band and the instrument. This observation suggests that the dictionary must be adapted to the different spectrometers. The results shown in Fig. S1 clearly illustrate the advantage of using SPIRIT for ISRF estimation, which leads to normalized estimation errors of less than 1%, significantly below those obtained using the parametric estimation methods. A comparison between the different sparse approximations (OMP, LASSO) and dictionaries (SVD, K-SVD) that can be used by SPIRIT shows that OMP often works better than LASSO also for these examples.

S3.2 Performance versus wavelength

Figs. S2 and S3 display performance results for all wavelengths as represented in the manuscript: spectral measurements and their reconstructions using the different methods, the absolute differences between the normalized spectral measurements and their normalized approximations (in logarithmic scale, second rows) and the associated residuals ρ, comparison between the ISRF approximation errors for different wavelengths (third rows), ISRF errors averaged over all the wavelengths as a function of the number of atoms selected from the dictionary (bottom rows). A collection of approximately 10% of the total number

[1]Data available at ftp://ftp.eumetsat.int/pub/EPS/out/GOME/Calibration-Data-Sets/Slit-Function-Key-Data/FM3-Metop-A/.
[2]Data available at https://www.knmiprojects.nl/projects/ozone-monitoring-instrument/data-products

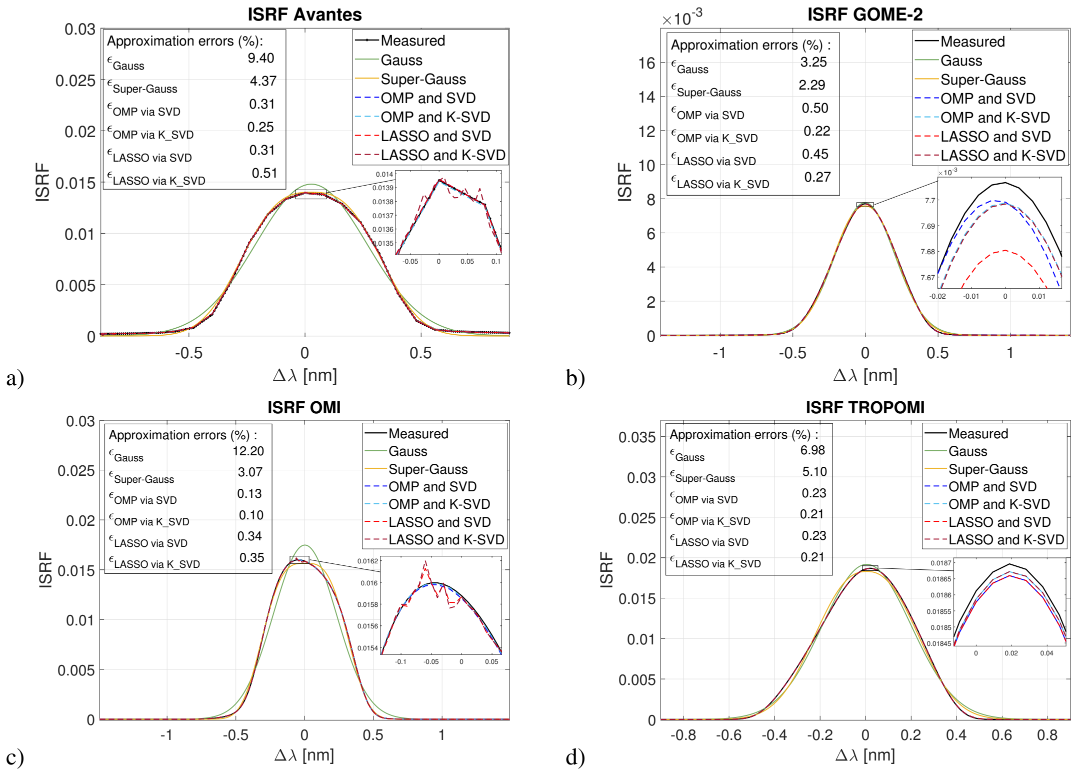

Fig. S1. Example of simulated ISRF for the spectrometers a) Avantes b) GOME-2 c) OMI and d) TROPOMI and its estimates using parametric methods and SPIRIT.

of ISRFs available was used for each instrument to estimate the dictionary. The number of atoms for the first three rows is determined as the value for K that minimizes the average ISRF error reported in the bottom row.

S3.2.1 Avantes

The measurements considered in this section correspond to the wavelengths ranging from 400 to 410 nm, to make a fair comparison with the results of (Beirle et al., 2017). The bottom plot of Fig. S2 (a) shows that $K = 5$ atoms is optimal for this instrument. Approximation errors for ISRF estimates using the Super-Gauss parameterization are lower than those obtained using the Gaussian model, which confirms the results of (Beirle et al., 2017). The proposed SPIRIT method allows us to obtain normalized errors less than 1%, which are significantly below those of parametric methods. The OMP algorithm tends to provide slightly better results than LASSO for this instrument. Note that the differences between using SVD and K-SVD for estimating the dictionary are found to be insignificant.

S3.2.2 GOME-2

The measurements considered in this paper have wavelengths ranging from 420 nm to 440 nm. The bottom plot of Fig. S2 (b) shows that choosing $K = 5$ atoms chosen from the dictionary leads to the best ISRF estimations. Inspection of the other rows of Fig. S2 (b) indicates again that the Super-Gauss parameterization performs better than the Gaussian one, but significantly worse than the proposed sparse representation. The K-SVD algorithm provides slightly better estimation results than SVD for this dataset, notably in the range 428 nm to 435 nm.

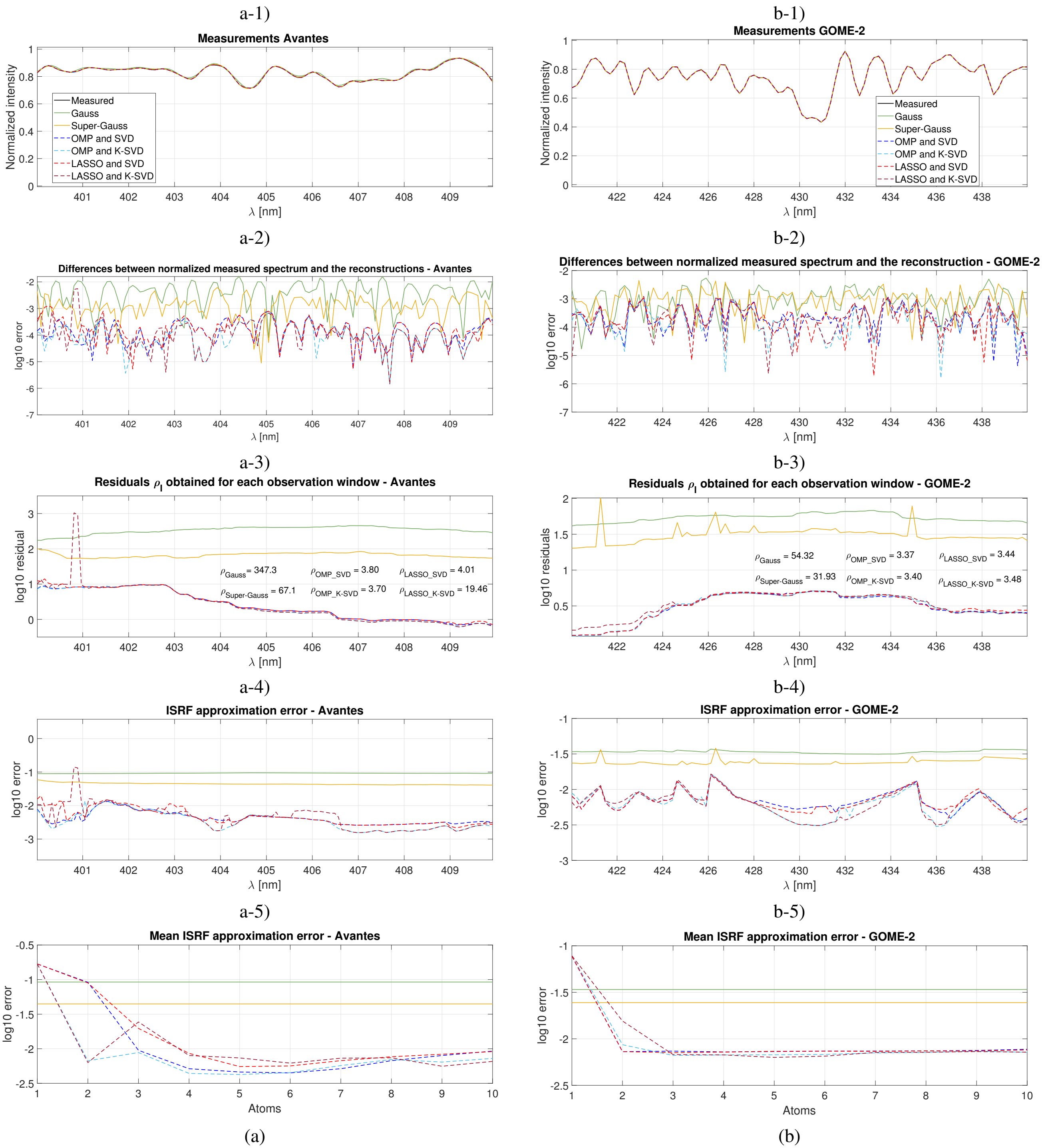

Fig. S2. Illustration of the measured spectrum (1), the difference between the measured spectrum and the reconstructed ones (2), the residuals ρ_l for each wavelengths (3), the ISRF approximation error versus the wavelength (4) and the mean ISRF approximation error versus the number of selected atoms (5) for different methods (Gauss, Super-Gauss, OMP, LASSO, SVD and KSVD) and for Avantes (a) and GOME-2 (b).

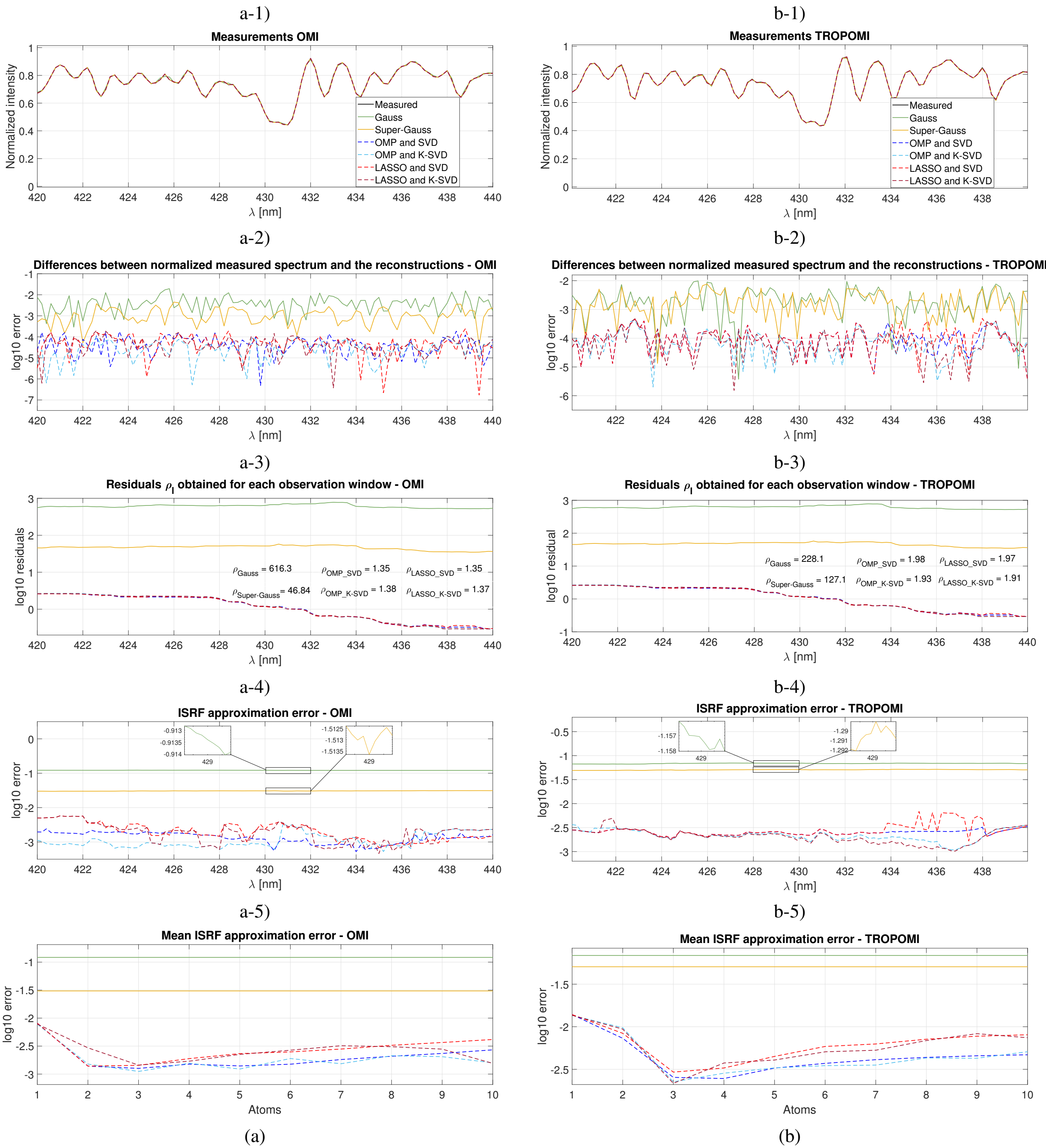

Fig. S3. Illustration of the measured spectrum (1), the difference between the measured spectrum and the reconstructed ones (2), the residuals ρ_l for each wavelengths (3), the ISRF approximation error versus the wavelength (4) and the mean ISRF approximation error versus the number of selected atoms (5) for different methods (Gauss, Super-Gauss, OMP, LASSO, SVD and KSVD) and for OMI (a) and TROPOMI (b).

S3.2.3 OMI

The measurement considered in this section are for wavelengths 420 to 440 nm as for the GOME-2 spectrometer. The measured spectrum is reconstructed with the sparse representation methods for $K = 5$ atoms chosen from the dictionary, which is estimated using SVD or K-SVD. For this spectrometer, Fig. S3 (a) highlights particularly well the importance of choosing a method other than the Gaussian model. The Super-Gaussian parameterization delivers better results in terms of measurement fit and ISRF approximation. However, methods based on sparse representation provide much better results, achieving mean approximation errors as low as 0.1%.

S3.2.4 TROPOMI

Fig. S3 (b) shows that sparse methods applied to TROPOMI data require a smaller number of atoms to minimize both the measurement fitting errors and the ISRF approximation errors. The proposed SPIRIT method yields significantly better performance than state-of-the-art parametric models, leading to more than one magnitude smaller ISRF approximation errors.

S3.2.5 Discussion

Overall, the conclusions from these experiments are as follows. First, the Super-Gaussian parameterization generally yields better performance than the Gaussian one, corroborating the results reported in (Beirle et al., 2017). However, the normalized ISRF approximation errors obtained with these parametric methods are consistently larger than 1%, for most instruments and wavelengths, contrary to the proposed SPIRIT approach based on sparse approximations of ISRFs in a suitable dictionary, which yields significantly better performance. This result is due to the fact that the ISRF shapes depend strongly on the spectrometer and can vary across wavelengths, which cannot be accommodated easily with a simple parametric model. On the contrary, decompositions in appropriate dictionaries that depend on the spectrometer and the chosen wavelength band offer sufficient flexibility for all use cases considered here. Regarding the estimation algorithms, SVD provides performance close to K-SVD except in some very specific cases, at significantly smaller cost. LASSO is usually outperformed by OMP. These results overall suggest the use of SVD for building the dictionary and OMP for ISRF estimation.

S3.3 Robustness to noise

To study the robustness of the different ISRF estimation methods to the presence noise, white Gaussian noise was added to the spectral measurements with several signal to noise ratio (SNR) levels. Table S2 reports the obtained residual approximation errors and the normalized average ISRF approximation errors for all instruments. Approximation errors less than $< 1\%$ are highlighted in blue. These results show that the proposed method yields normalized errors below 1% for SNR larger than 20 dB. Note that the use of LASSO for sparse coding leads to larger errors than the use of OMP for all spectrometers, again leading to the recommandation of using OMP instead of LASSO. The proposed ISRF estimation methods globally yield the smallest approximation and residual errors, hence the best estimation results. Note that the errors obtained with the parametric models do not vary significantly with the noise level, except for the smallest SNR, indicating that errors due to model misfit are larger than those induced by the noise degradations. To conclude, OMP combined with SVD provides the overall best results for ISRF estimation, also in the presence of additive noise.

S4 Conclusions

In conclusion, this supplementary material extends the application of sparse representation-based methods for estimating ISRFs to four additional spectrometers, demonstrating the broader applicability and strong performance of the proposed algorithms on instruments beyond those used in the main manuscript. The findings indicate that the method is robust across four different design choices, yielding consistent results. Overall, the results support the use of SVD for dictionary construction and OMP for ISRF estimation.

Table S2. Mean ISRF approximation errors and residuals for different SNRs and different methods (Gauss (G), Super-Gauss (SG), OMP and LASSO, SVD and K-SVD).

Instrument	/ SNR	Mean ISRF approximation error (%)						Residual error					
		G	SG	OMP SVD	OMP K-SVD	LASSO SVD	LASSO K-SVD	G	SG	OMP SVD	OMP K-SVD	LASSO SVD	LASSO K-SVD
Avantes	20 dB	9.27	4.78	**3.06**	3.30	6.04	5.89	645.5	351.7	271.1	**270.3**	311.1	303.2
	40 dB	9.22	4.45	**0.50**	0.51	0.80	0.83	351.2	70.06	6.50	**6.40**	15.21	15.13
	55 dB	9.22	4.45	0.46	**0.43**	0.65	0.65	347.6	67.23	3.87	**3.78**	12.64	12.58
	80 dB	9.22	4.45	0.46	**0.42**	0.65	0.64	347.3	67.12	3.79	**3.70**	12.57	12.49
GOME-2	20 dB	3.47	2.76	2.63	2.54	2.61	**2.38**	342.1	321.2	**264.4**	265.8	266.3	269.1
	40 dB	3.39	2.49	0.72	**0.65**	0.74	**0.65**	57.26	37.45	**6.04**	6.08	6.08	6.25
	55 dB	3.39	2.46	0.69	0.59	0.69	**0.58**	54.42	32.79	**3.42**	3.50	3.46	3.62
	80 dB	3.39	2.44	0.69	**0.58**	0.69	**0.58**	54.32	30.33	**3.33**	3.42	3.38	3.53
OMI	20 dB	12.18	3.30	**2.71**	2.95	6.48	6.68	904.6	329.3	261.4	265.6	**255.5**	259.3
	40 dB	12.17	3.06	0.30	**0.28**	0.68	0.71	619.0	49.39	3.97	4.04	**3.94**	3.97
	55 dB	12.17	3.06	0.15	**0.12**	0.26	0.26	616.4	46.88	**1.43**	1.46	**1.43**	1.45
	80 dB	12.17	3.06	0.15	**0.11**	0.25	0.24	616.3	46.84	**1.35**	1.38	**1.35**	1.37
TROPOMI	20 dB	6.88	5.16	**2.16**	2.17	3.39	3.42	517.6	410.9	**273.9**	275.1	274.2	276.5
	40 dB	6.87	5.07	**0.30**	0.34	0.41	0.38	230.9	129.7	4.70	4.74	4.69	**4.61**
	55 dB	6.87	5.07	**0.25**	0.26	0.33	0.33	228.2	127.1	2.04	2.05	2.02	**1.96**
	80 dB	6.87	5.07	**0.25**	0.26	0.34	0.33	228.1	127.1	1.96	1.99	1.95	**1.88**

References

AvaSpec-ULS2048x64-EVO - Data User's product description, https://avantes.b-cdn.net/content/uploads/2020/11/DS-Spec-Avaspec-ULS2048x64-EVO-200702.pdf(lastaccess:06November2023).

Babic, L., Braak, R., Dierssen, W., Kissi-Ameyaw, J., Kleipool, Q., Leloux, J., Loots, E., Ludewig, A., Rozemeijer, N., Smeets, J., and Vacanti, G.: Algorithm theoretical basis document for the TROPOMI L01b data processor, sentinels.copernicus.eu/documents/247904/2476257/Sentinel-5P-TROPOMI-Level-1B-ATBD, 2022.

Beirle, S., Lampel, J., Lerot, C., Sihler, H., and Wagner, T.: Parameterizing the instrumental spectral response function and its changes by a super-Gaussian and its derivatives, Atmos. Meas. Tech., 10, 581–598, https://doi.org/10.5194/amt-10-581-2017, 2017.

Dobber, M. R., Dirksen, R. J., Levelt, P. F., van den Oord, G. H. J., Voors, R. H. M., Kleipool, Q., Jaross, G., Kowalewski, M., Hilsenrath, E., Leppelmeier, G. W., de Vries, J., Dierssen, W., and Rozemeijer, N. C.: Ozone monitoring instrument calibration, IEEE Trans. Geosci. Remote Sens., 44, 1209–1238, https://doi.org/10.1109/TGRS.2006.869987, 2006.

El Haouari, J., Gaucel, J.-M., Pittet, C., Tourneret, J.-Y., and Wendt, H.: In-Flight Estimation of Instrument Spectral Response Functions Using Sparse Representations., in: Atmos. Meas. Tech., preprint, 2024.

Kleipool, Q., Ludewig, A., Babić, L., Bartstra, R., Braak, R., Dierssen, W., Dewitte, P.-J., Kenter, P., Landzaat, R., Leloux, J., Loots, E., Meijering, P., van der Plas, E., Rozemeijer, N., Schepers, D., Schiavini, D., Smeets, J., Vacanti, G., Vonk, F., and Veefkind, P.: Pre-launch calibration results of the TROPOMI payload on-board the Sentinel-5 Precursor satellite, Atmos. Meas. Tech., 11, 6439–6479, https://doi.org/10.5194/amt-11-6439-2018, 2018.

Munro, R., Lang, R., Klaes, D., Poli, G., Retscher, C., Lindstrot, R., Huckle, R., Lacan, A., Grzegorski, M., Holdak, A., Kokhanovsky, A., Livschitz, J., and Eisinger, M.: The GOME-2 instrument on the Metop series of satellites: instrument design, calibration, and level 1 data processing – an overview, Atmos. Meas. Tech., 9, 1279–1301, https://doi.org/10.5194/amt-9-1279-2016, 2016.

Schenkeveld, V. M. E., Jaross, G., Marchenko, S., Haffner, D., Kleipool, Q. L., Rozemeijer, N. C., Veefkind, J. P., and Levelt, P. F.: In-flight performance of the Ozone Monitoring Instrument, Atmos. Meas. Tech., 10, 1957–1986, https://doi.org/10.5194/amt-10-1957-2017, 2017.

Siddans, R. and Latter, B. G.: Analysis of GOME-2 (FM201-3): Slit function Measurements Final Report Eumetsat Contract No. EUM/CO/04/1298/RM, https://www.eumetsat.int/media/42779, 2018.

Smeets, J., Kleipool, Q., van Hees, R., and M., S.: Readme for TROPOMI instrument spectral response functions, https://sentinels.copernicus.eu/documents/247904/3541451/S5P-KNMI-OCAL-0149-ME-readme_for_TROPOMI_UVN_instrument_spectral_response_function-3.0.0-20180401_0.pdf, 2002.

Sun, K., Liu, X., Huang, G., González Abad, G., Cai, Z., Chance, K., and Yang, K.: Deriving the slit functions from OMI solar observations and its implications for ozone-profile retrieval, Atmos. Meas. Tech., 10, 3677–3695, https://doi.org/10.5194/amt-10-3677-2017, 2017.

van Hees, R. M., Tol, P. J. J., Cadot, S., Krijger, M., Persijn, S. T., van Kempen, T. A., Snel, R., Aben, I., and Hoogeveen: Determination of the TROPOMI-SWIR instrument spectral response function, Atmospheric Measurement Techniques, 11, 3917–3933, https://doi.org/10.5194/amt-11-3917-2018, 2018.